Available online at www.sciencedirect.com
ScienceDirect
Advances in Space Research 41 (2008) 2112–2117
ADVANCES IN SPACE RESEARCH (a COSPAR publication)
www.elsevier.com/locate/asr

Comparative study of the influence of natural convection on directional solidification of Al–3.5 wt% Ni and Al–7 wt% Si alloys

B.H. Zhou [a,b], H. Jung [a], N. Mangelinck-Noël [a], H. Nguyen-Thi [a], B. Billia [a,*], Q.S. Liu [b], C.W. Lan [c]

[a] L2MP, UMR 6137, Université Paul Cézanne (Aix-Marseille III), Marseille, France
[b] Institute of Mechanics, NML/CAS, Chinese Academy of Sciences, Beijing, China
[c] Department of Chemical Engineering, National Taiwan University, Taipei, China

Received 23 October 2006; received in revised form 10 May 2007; accepted 18 June 2007

Abstract

We present numerical simulations of thermosolutal convection for directional solidification of Al–3.5 wt% Ni and Al–7 wt% Si. Numerical results predict that fragmentation of dendrite arms resulting from dissolution could be favored in Al–7 wt% Si, but not in Al–3.5 wt% Ni. Corresponding experiments are in qualitative agreement with the numerical predictions. Distinguishing the two fragmentation mechanisms, namely dissolution and remelting, is critical during experiments on earth, when fluid flow is dominant.

Keywords: Solidification; Mushy zone; Natural convection; Dendrite fragmentation

1. Introduction

During directional solidification of binary alloys, melt convection influences both the macro/micro segregations and microstructure formation. Even when solidification is performed in a thermal (i.e. vertical upward solidification) and solutal (i.e. rejected solute denser than solvent) stabilizing configuration, convection in the melt driven by radial thermal gradient can be strong when the growth rate is slow enough. As a consequence of convection, a large macroscopic deformation of the front and associated radial non-uniformity of the microstructure are observed (Nguyen-Thi et al., 2005).

A first numerical model was proposed using front-tracking method to capture the liquid–solid interface but flow penetration in the dendritic mushy zone was neglected. Despite this strong simplification, numerical simulations explained the microstructure localisation phenomena (i.e. cell/dendrite cluster in the center with eutectic at the periphery) (Nguyen-Thi et al., 2006).

However, it is well known that interdendritic convection interacts directly with solidification microstructure in the mushy zone, leading to changes in primary and secondary spacings or formation of freckles (segregated channels filled with dendrite fragments). Macrosegregation caused by convection in the mushy zone can be interpreted through the so-called 'local solute redistribution equation' (LSRE), proposed by Flemnings et al. in the sixties (Flemings, 2000). An important deduction of LSRE is that solute-rich melt will cause local dissolution (or remelting) of dendrites, when flow velocity is in the direction of increasing temperature and larger than isotherm velocity, in the reference frame of the crucible (Beckermann, 2002). When dendrite fragments formed by this local dissolution mechanism are carried into the bulk melt, they could promote columnar to equiaxed transition (CET) where local undercooling condition is favorable (Hellawell et al., 1997; Campanella et al., 2003; Spittle, 2006).

* Corresponding author.
E-mail addresses: binghong.zhou@L2MP.fr (B.H. Zhou), bernard.billia@L2MP.fr (B. Billia).

0273-1177/$34.00
doi:10.1016/j.asr.2007.06.038

A classical approach of solidification modelling is to treat the liquid and mushy regions in separate domains. The fluid motion in the melt region is modelled in general by the Navier–Stokes equations, while that within the mushy is modelled as in a porous medium (Darcy's law). The first solidification model using the multi-domain method was reported in Ridder et al. (1981). He considered an axi-symmetric ingot but did not take into account the solutal convection and the crucible. Worster et al. and others (Worster, 1997) used an idealized two-dimensional model to study the dynamical interaction between fluid and mushy zone. Another approach called one-domain model or continuum model, is widely used in the casting community to simulate freckles formation (Beckermann, 2002).

In this study, we adopt the multi-domain approach to extend our numerical model of directional solidification to consider the fluid flow penetration in the mushy zone. Two aluminium-based alloys, Al–3.5 wt% Ni and Al–7.0 wt% Si, are investigated through numerical simulations as well as solidification experiments. It will be shown that these two alloys exhibit different macrosegregation behavior and microstructure formation. The experimental observations can be well interpreted using the predictions of numerical modeling.

2. Mathematical formulation

The generic representation of upward directional solidification in a cylindrical crucible is illustrated in Fig. 1. An alloy of initial concentration C_0 is pulled down in a Bridgman furnace. The furnace is described by an effective heating profile $T_a(z)$, with a temperature gradient G in the middle part. A quasi-steady-state with a pulling rate V_p ($\boldsymbol{V}_p = -V_p\,\boldsymbol{k}$, where $\boldsymbol{k}$ is a unit vector in the vertical z-direction.) larger than critical velocity of Mullins–Sekerka instability is considered here, so that a mushy zone of solid dendrites surrounded by a liquid phase is formed. In this configuration, the mushy zone is sandwiched between the melt region above and the completely solid region below.

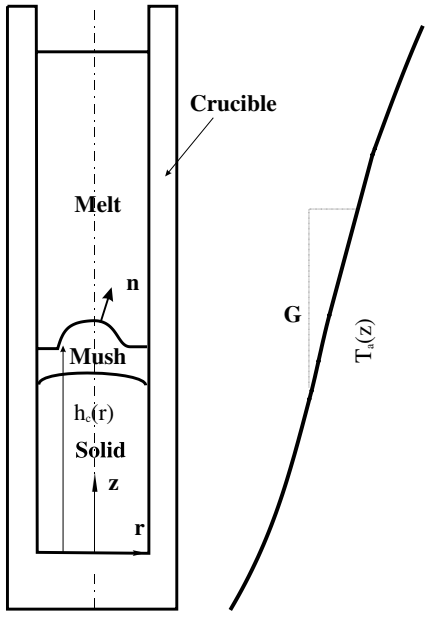

Fig. 1. Schematic representation of directional solidification in a cylindrical crucible, the actual temperature profile $T_a(z)$ is imposed at the outside crucible wall.

We invoke the following assumptions in the mushy zone (Worster, 1997): (1) there is thermal equilibrium (no undercooling); (2) the densities of solid and liquid are equal (no solid shrinkage); (3) the mushy zone behaves as an isotropic and uniform porous medium in which the flow is governed by Darcy's equation. The last uniformity assumption is a first order simplification and it is supported by direct observation of the mushy zone by using the quenching technique (see Fig. 2(a) in Nguyen-Thi et al. (2006)). In this paper, we simply describe the dimensional control equations in the reference frame of laboratory, and the method used to determine the mush-liquid interface. A comprehensive presentation and discussion of our model will appear in a subsequent paper.

In the melt, Boussinesq approximation is used to describe fluid flow. Control equations for conservation laws of mass, momentum, solute and energy are as follows:

$$\nabla \cdot \boldsymbol{V} = 0 \tag{1}$$

$$(\boldsymbol{V} + \boldsymbol{V}_p)\cdot\nabla\boldsymbol{V} = -\frac{1}{\rho_0}\nabla p + \nu\nabla^2\boldsymbol{V} - [\beta_T(T - T_0) + \beta_c(C - C_0)]\mathbf{g} \tag{2}$$

$$(\boldsymbol{V} + \boldsymbol{V}_p)\cdot\nabla C = D\nabla^2 C \tag{3}$$

$$(\boldsymbol{V} + \boldsymbol{V}_p)\cdot\nabla T = \frac{\chi_l}{\rho_0 c_{pl}}\nabla^2 T \tag{4}$$

where $\boldsymbol{V}$ is the fluid velocity viewed in the reference frame of the crucible ($\boldsymbol{V} + \boldsymbol{V}_p$ is the fluid velocity in the laboratory frame), ρ_0 is a reference density of liquid as well as solid, ν is the kinematic viscosity of melt, $\beta_T = -\frac{1}{\rho_0}\frac{\partial\rho}{\partial T}$ and $\beta_c = -\frac{1}{\rho_0}\frac{\partial\rho}{\partial C}$ are thermal and solutal expansion coefficient respectively, $\mathbf{g}$ is the gravity acceleration, D the solute diffusivity, χ the thermal conductivity and c_p the specific heat capability.

In the mushy zone, the solute concentration can be determined from temperature through the assumption of local thermodynamic equilibrium

$$T = T_M + mC \tag{5}$$

where T_M is the melting temperature of pure aluminum and m the slope of the liquidus. The equations governing conservation of heat and momentum are

$$(\boldsymbol{V} + \boldsymbol{V}_p)\cdot\nabla T = \frac{\chi_m}{\rho_0 c_{pm}}\nabla^2 T \tag{6}$$

$$\frac{\nu}{K}\boldsymbol{V} = -\frac{1}{\rho_0}\nabla p - [\beta_T(T - T_0) + \beta_c(C - C_0)]\mathbf{g} \tag{7}$$

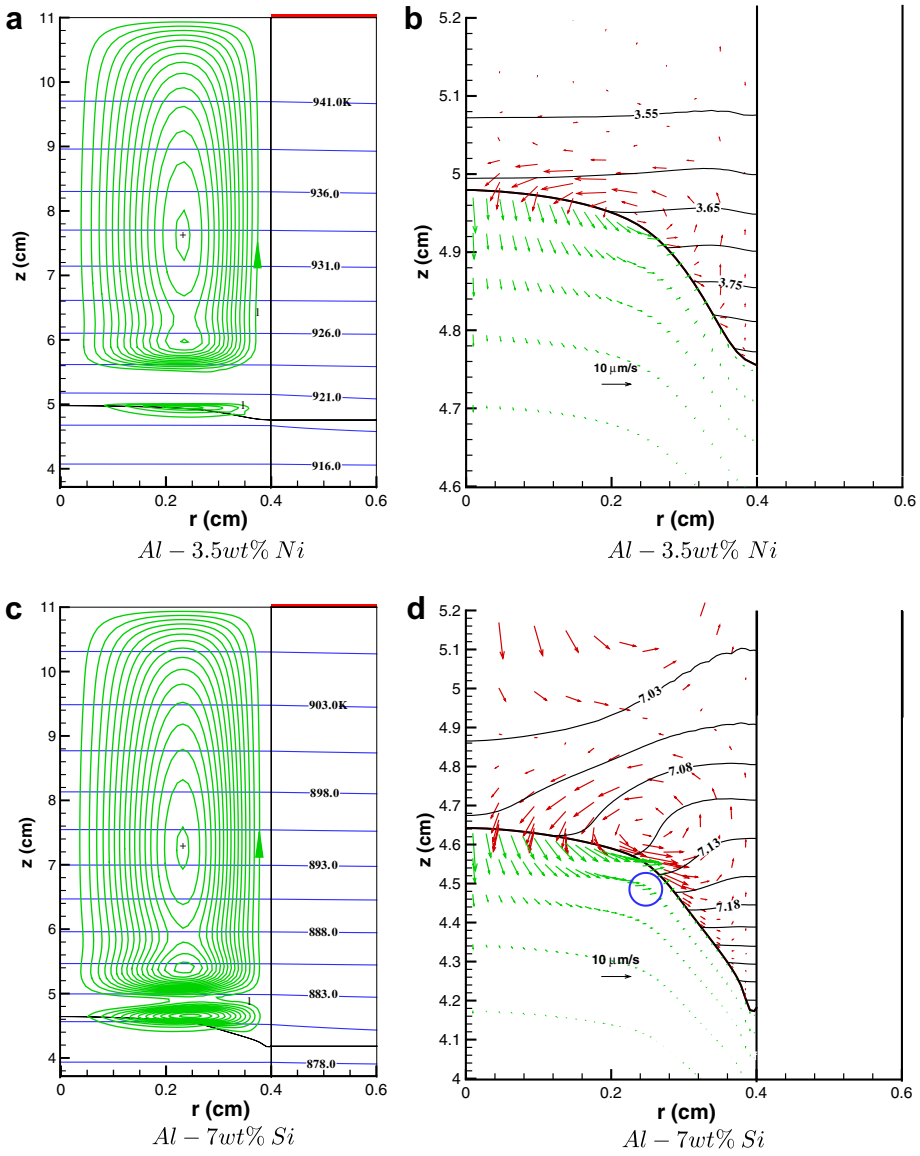

Fig. 2. Numerically simulated temperature, solute and flow fields for Al-based alloys ($G = 5$ K/cm, $V_p = 2$ μm/s), (a) and (c): global convection pattern and temperature distribution, the contour value marked with *1* and increment are both 2.5×10^{-6} cm^3/s; (b) and (d): solute distribution (solid line, in wt%) and flow field nearby the mush-melt interface (arrows).

where the subscripts m and l mean mush and liquid respectively, K is the permeability of the mushy zone and it is estimated as 1.0×10^{-12} m^2 for both alloys.

The control equations for temperature distribution in the solid and the crucible have the same form:

$$\boldsymbol{V}_p \cdot \nabla T = \frac{\chi_i}{\rho_i c_{pi}} \nabla^2 T \tag{8}$$

where $i = s$ or c, represents the solid and the crucible respectively.

The above mentioned control equations should be closed with appropriate boundary and connection conditions. These conditions can be found in Lan and Chen (1996) and Worster (1997). Especially, the liquid fraction is calculated through the solute conservation at the mush-solid interface. As the mushy zone (that can be viewed as the consequence of morphological instability), acts to reduce the region of constitutional supercooling in the system, we adopt here the suggestion in Worster (1997) of marginal equilibrium at the mush-liquid interface. In other words, the normal temperature gradient at the mush-liquid interface is equal to the normal gradient of equilibrium temperature (linear with concentration):

$$\nabla T_l \cdot \mathbf{n} = m \nabla C_l \cdot \mathbf{n} \tag{9}$$

We use a finite volume method to discretize the control equations on a boundary-fitted coordinate system. After that, the obtained set of non-linear algebraic equations is solved by Newton's method to get the solution of the solidification problem (Lan and Chen, 1996). The validation of the computer code has been confirmed by reproducing the Fig. 3 in Lan and Tu (2000), when we

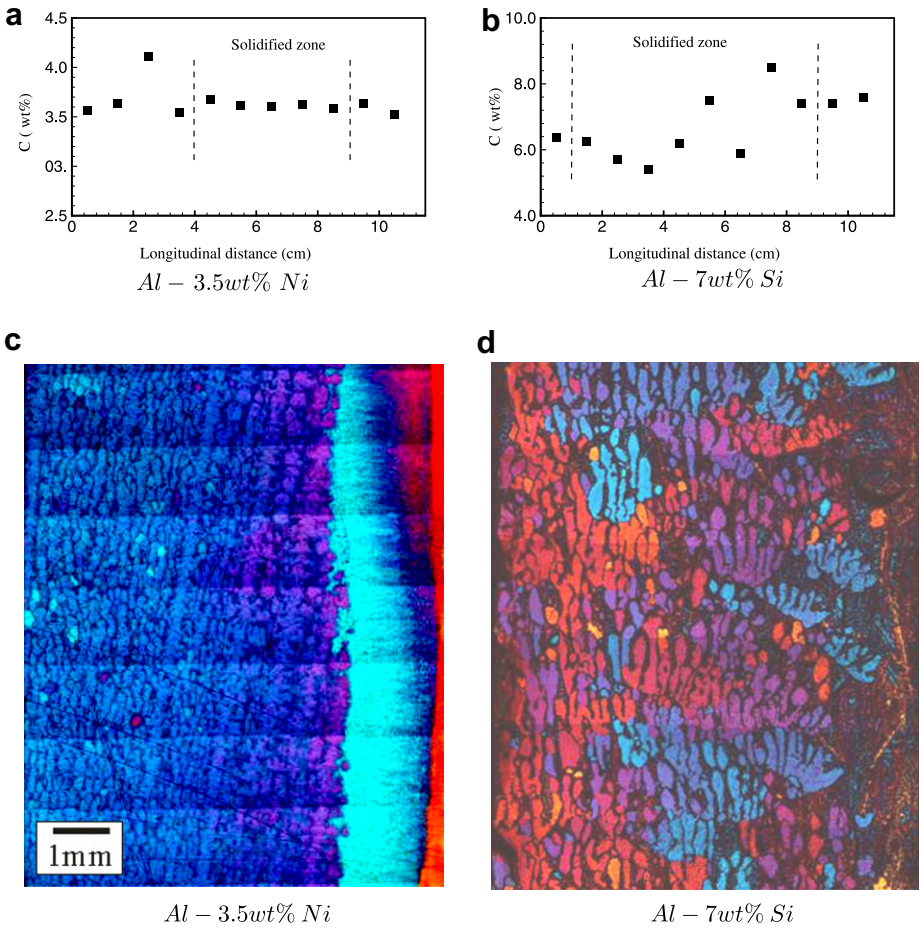

Fig. 3. (a,b) Longitudinal macrosegregations of solute; (c,d) microstructure in longitudinal section after anodization treatment, $G = 5$ K/cm, $V_p = 2$ μm/s.

set the mushy zone as full solid. There are 60×90 finite volumes in the melt and 60×50 in the mush. Grid distribution and other details on numerical method can be found in Lan and Tu (2000).

3. Numerical results and microstructure prediction

Numerical simulations were carried out on two Al-based alloys, Al–3.5 wt% Ni and Al–7 wt% Si (Table 1) corresponding to the processing condition of our solidification experiments. For the sake of simplicity, numerical and experimental results will be compared at a pulling rate of 2 μm/s and temperature gradient of 5 K/cm. The solidification cylindrical sample of 0.8 cm in diameter and 11 cm in length is simulated in this paper. The numerical results are illustrated in Fig. 2. The convection patterns in the two alloy systems are roughly the same: both consist of two co-rotating rolls (i.e. a large one in the bulk liquid and a small one in the region adjacent to the mush-liquid interface), with liquid moving downward at the centerline and upward along the crucible wall (Fig. 2(a) and (c)). This global convection pattern is consistent with our previous simulation (Nguyen-Thi et al., 2006), which neglected the penetration effect in the mush, and also shows agreement with (Mazumder and Trivedi, 2004). The driving force of convection in the melt is the radial thermal gradient due to the thermal mismatch between melt, solid and crucible (i.e. the thermal conductivity of solid is larger than the thermal conductivity of the melt and much larger than that of the crucible, see the detailed discussion in (Mazumder and Trivedi, 2004). The maximum temperature difference between the edge and the center of the sample is 0.32 K (at $z = 4.98$ cm) for Al–3.5 wt% Ni, and 0.24 K (at $z = 4.64$ cm) for Al–7.0 wt% Si. Subsequently, solutal effect increases the magnitude of the front deformation.

Although the global convection pattern is similar for both alloys, significant differences can be found when we focus on the interaction between convection and solute distribution. For Al–3.5 wt% Ni, the two co-rotating convective rolls are completely separated by a nearly static region about 5 mm high. Furthermore, the lower small roll is well confined to the solute boundary layer and the mushy zone below, while the large roll is limited in the bulk melt with uniform concentration of C_0. This indicates that stationary growth can be achieved and no longitudinal macrosegregation is expected in the sample. On the other hand, a small part of the large convection roll in the bulk liquid region penetrates into the solute boundary layer in the case of Al–7 wt% Si, so that a weak longitudinal macrosegregation is expected.

Table 1
Physical properties used in the simulation

Description	Al–3.5 wt% Ni	Al–7.0 wt% Si
Density, ρ_0	2.37×10^3 kg/m^3	2.37×10^3 kg/m^3
Thermal conductivity of solid, χ_s	0.221 kJ/(Km s)	0.221 kJ/(Km s)
Thermal conductivity of liquid, χ_l	0.107 kJ/(Km s)	0.107 kJ/(Km s)
Specific heat of solid, c_{ps}	0.124 kJ/(kg K)	0.124 kJ/(kg K)
Specific heat of liquid, c_{pl}	0.124 kJ/(kg K)	0.124 kJ/(kg K)
Melting point of pure Al, T_M	932.4 K	932.4 K
Heat of fusion, ΔH	4.0×10^2 kJ/kg	4.0×10^2 kJ/kg
Liquidus slope, m	-3.5 K (wt%)$^{-1}$	-7.3 K (wt%)$^{-1}$
Segregation coefficient, k	0.004	0.13
Eutectic concentration, C_E	5.7 wt%	12.6 wt%
Thermal expansion coefficient, β_T	1.0×10^{-4} K^{-1}	1.0×10^{-4} K^{-1}
Solutal expansion coefficient, β_c	-2.5×10^{-2} (wt%)$^{-1}$	-4.0×10^{-4} (wt%)$^{-1}$
Solutal diffusivity, D	2.2×10^{-9} m^2 s^{-1}	3.0×10^{-9} m^{2}s^{-1}
Kinematic viscosity, v	4.0×10^{-7} m^{2}s^{-1}	4.0×10^{-7} m^{2}s^{-1}
	Crucible (Boron Nitride)	
Density, ρ_c	1.90×10^3 kg/m^3	
Thermal conductivity, χ_c	0.025 kJ/(Km s)	
Specific heat, c_{pc}	0.18 kJ/(kg K)	

During directional solidification, the influence of interdendritic liquid flow on microstructure can be understood through the following 'local solute redistribution equation' (LSRE):

$$-\frac{\partial f_l}{\partial C_l}=\frac{1-\beta}{1-k}\left(1-\frac{V_z}{V_p}\right)\frac{f_l}{C_l} \tag{10}$$

where f_l is the liquid volume fraction; C_l the liquid concentration; $\beta=\frac{\rho_s-\rho_l}{\rho_s}$ the solidification shrinkage; k the partition coefficient and V_z is the vertical liquid velocity. A detailed discussion on the physical significance of LSRE can be found in (Flemings, 2000; Beckermann, 2002). In diffusive solidification process ($V_z=0$), LSRE reduces to the well known Scheil equation. The influence of interdendritic flow can be characterized by a non-dimensional convective parameter $\Gamma=\frac{V_z}{V_p}$. An important deduction of LSRE is that dissolution (local remelting) occurs when $\Gamma>1$. By inserting this relation in LSRE, it is readily seen that, when the solute concentration increases (and so local temperature decreases), local dissolution occurs rather than solidification, i.e., $\frac{\partial f_l}{\partial C_l}$ becomes positive and therefore $\frac{\partial f_l}{\partial T_l}$ becomes negative (using relation (5) and noting that $\frac{\partial f_l}{\partial T_l}>0$ means solidification). This is called dissolution rather than remelting in the literature (Flemings, 2000; Beckermann, 2002), because 'local solute redistribution' directly translates into local supersaturation in this process.

It follows from numerical results that the maximum value of the convective parameters in our calculation are $\Gamma=0.45$ for Al–3.5 wt% Ni and $\Gamma=1.2$ for Al–7 wt% Si. It is worth noticing that, in Al–7 wt% Si, $\Gamma>1$ happens in a small region with $0.25<r<0.28$ and $4.48<z<4.54$ (cm) (indicated by the circle in Fig. 2(d)). This implies that dendrite arm dissolution can happen in Al–7 wt% Si alloy but not in Al–3.5 wt% Ni, with $G=5$ K/cm and $V_p=2$ μm/s. These numerical predictions are consistent with our experimental observations as discussed in Section 4.

4. Experimental solidification results

Directional solidification experiments are achieved in a Brigdgman-type furnace, see Jung et al. (2006) for details. Both alloys are solidified with a pulling rate of $V_p=2$ μm/s and a temperature gradient $G=5$ K/cm. Axial composition profile is determined by chemical analysis of thin slices of 500 μm width cut all along the solidified samples. Solidification microstructure is revealed on longitudinal sections by mechanical polishing first, and then anodization treatment (electrochemical etching). With the later technique, grains with different crystallographic orientations are marked with different colors when seen under a polarized microscope.

As shown in Fig. 3(a) and (b), solute macrosegregation in longitudinal direction is quite different for the two alloys. For Al–3.5 wt% Ni, the Ni concentration is uniform in the solidified zone and almost no longitudinal segregation is observed. For Al–7 wt% Si, however, a weak longitudinal Si macrosegregation is measured in the solidified region. As mentioned in the previous section, this can be well explained by referring to the different interaction between convection in the bulk liquid and fluid flow in the solute boundary layer (see Fig. 2(a) and (c)).

Moreover, microstructure difference between these two alloys is evident. As can be seen in Fig. 3(c), Al–3.5 wt% Ni alloy exhibits a fully columnar dendritic microstructure, with a strip of eutectic on the right (This originates from a slight misalignment of the crucible with the axis of the furnace). Unlike Al–3.5 wt% Ni, for Al–7 wt% Si (Fig. 3(d)), there is a large band of equiaxed-like dendrites appearing between a strip of eutectic on the right and columnar dendrites on the left side (Microstructure is not axisymmetric for the same reason as before). This is consistent with numerical prediction: conditions for dendrite arm fragmentation by dissolution are satisfied in Al–7 wt% Si but not in Al–3.5 wt% Ni solidification. After fragmentation, the dendrite fragments are likely to settle down and rotate due to gravity, because the density of dendrites (solid) is larger than the melt (Reinhart et al., 2005). This would result in different orientations of dendrite arms exhibiting different colors after anodization treatment, as it is observed for Al–7 wt% Si.

5. Conclusion and discussion

In summary, even for directional solidification in both thermal and solutal stabilizing situation, natural convection initiated by radial thermal gradient influences the solidification process markedly. This article shows that natural convection in the mushy zone is indeed a major factor in

dendrite arm fragmentation due to local dissolution effect. On earth, it is difficult to distinguish between the two often discussed dendrite remelting mechanisms (Li et al., 2004; Mathiesen et al., 2006): local pileup of solute in the mush by fluid convection (dissolution) and thermal recalescence caused by the solidification latent heat (remelting). Dedicated careful experimental studies in the microgravity environment of space are needed, in order to further clarify the mechanism of fragmentation by suppressing the effects of buoyancy. Conversely, fragmentation induced by convection in the mushy zone should be characterized during directional solidification on earth (Flemings, 2000; Beckermann, 2002; Campanella et al., 2003).

Furthermore, it should be pointed out that fragmentation is a microscale phenomenon whereas the interaction of interdendritic flow with dissolution and remelting process has to be considered in a complete global model. However, numerical simulations on the macroscale of solidification together with such microscale model is not available at present time, and not foreseen in a near future (Beckermann, 2002). Therefore, numerical simulation based on macroscale model still serves as an important method to gain insight on the microscale effects of fluid flow in the mushy zone.

References

Beckermann, C. Modelling of macrosegregation: applications and future needs,2002. Int. Mat. Rev. 47, 243–261, 2002.

Campanella, T., Charbon, C., Rappaz, M. Influence of permeability on the grain refinement induced by forced convection in copper-base alloys. Scripta Mater. 49 (10), 1029–1034, 2003.

Flemings, M.C. Our understanding of macrosegregation: past and present. ISIJ Int. (Japan) 40 (9), 833–841, 2000.

Hellawell, A., Liu, S., Lu, S.Z. Dendrite fragmentation and the effects of fluid flow in castings. JOM 49 (3), 18–20, 1997.

Jung, H., Mangelinck-Noël, N., Nguyen-Thi, H., Billia, B. Columnar to equiaxed transition in directional solidification processing of aluminium alloys. Modeling of casting, welding and advanced solidification processes–XI, TMS, 399–406, 2006.

Lan, C.W., Chen, F.C. A finite volume method for solute segregation in directional solidification and comparison with a finite element method. Comput. Method. Appl. Mech. Engrg. 131, 191–207, 1996.

Lan, C.W., Tu, C.Y. Morphological instability due to double diffusive convection in directional solidification: the pit formation. J. Cryst. Growth 220 (4), 619–630, 2000.

Li, B., Brody, H.D., Kazimirov, A. Real-time observation of dendrite coarsening in Sn–13%Bi alloy by synchrotron microradiography. Phys. Rev. E 7006 (6), 2602, 2004.

Mathiesen, R.H., Arnberg, L., Bleuet, P., Somogyi, A. Crystal fragmentation and columnar-to-equiaxed transitions in Al–Cu studied by synchrotron X-ray video microscopy. Metallurg. Mater. Trans. A 37, 2515–2524, 2006.

Mazumder, P., Trivedi, R. Integrated simulation of thermo-solutal convection and pattern formation in directional solidification. Appl. Mathemat. Modell. 28 (1), 109–125, 2004.

Nguyen-Thi, H., Dabo, Y., Drevet, B., Dupouy, M.D., Camel, D., Billia, B., Hunt, J.D., Chilton, A. Directional solidification of Al–1.5 wt% Ni alloys under diffusion transport in space and fluid-flow localisation on earth. J. Cryst. Growth 281 (2-4), 654–668, 2005.

Nguyen-Thi, H., Zhou, B.H., Reinhart, G., Billia, B., Liu, Q.S., Lan, C.W., Lyubimova, T., Roux, B. Influence of forced convection on columnar microstructure during directional solidification of Al–Ni alloys. Mat. Sci. Forum 508, 181–186, 2006.

Reinhart, G., Mangelinck-Noel, A., Nguyen-Thi, H., Schenk, T., Gastaldi, J., Billia, B., Pino, P., Hartwig, J., Baruchel, J. Investigation of columnar-equiaxed transition and equiaxed growth of aluminium based alloys by X-ray radiography. Mat. Sci. Eng. A 413, 384–388, 2005.

Ridder, S.D., Kou, S., Mehrabian, R. Effect of fluid flow on macrosegregation in axisymmetric ingots. Metall. Trans. B. 12 (3), 435–447, 1981.

Spittle, J.A. Columnar to equiaxed grain transition in as solidified alloys. Int. Mat. Rev. 51, 247–269, 2006.

Worster, M.G. Convection in mushy layers. Annu. Rev. Fluid Mech. 29, 91–122, 1997.